Inorg. Chem. **2008**, *47*, 4032−4044

Interaction of Molecular Hydrogen with Open Transition Metal Centers for Enhanced Binding in Metal-Organic Frameworks: A Computational Study

Rohini C. Lochan, Rustam Z. Khaliullin, and Martin Head-Gordon*

Department of Chemistry, University of California and Chemical Sciences Division, Lawrence Berkeley National Laboratory, Berkeley, California 94720

Received August 16, 2007

Molecular hydrogen is known to form stable, "nonclassical" sigma complexes with transition metal centers that are stabilized by donor–acceptor interactions and electrostatics. In this computational study, we establish that strong H_2 sorption sites can be obtained in metal-organic frameworks by incorporating open transition metal sites on the organic linkers. Using density functional theory and energy decomposition analysis, we investigate the nature and characteristics of the H_2 interaction with models of exposed open metal binding sites {half-sandwich piano-stool shaped complexes of the form (Arene)$ML_{3-n}(H_2)_n$ [M = Cr, Mo, V^-, Mn^+; Arene = C_6H_5X (X = H, F, Cl, OCH_3, NH_2, CH_3, CF_3) or $C_6H_3Y_2X$ (Y = COOH, X = CF_3, Cl; L = CO; n = 1–3]}. The metal−H_2 bond dissociation energy of the studied complexes is calculated to be between 48 and 84 kJ/mol, based on the introduction of arene substituents, changes to the metal core, and of charge-balancing ligands. Thus, design of the binding site controls the H_2 binding affinity and could be potentially used to control the magnitude of the H_2 interaction energy to achieve reversible sorption characteristics at ambient conditions. Energy decomposition analysis illuminates both the possibilities and present challenges associated with rational materials design.

I. Introduction

One of the key challenges in the development of a hydrogen-based economy for transportation applications is the efficient, safe, and economical on-board storage of hydrogen in automobiles.[1–4] Microporous metal-organic frameworks (MOFs) are one of the recently introduced, potential hydrogen storage material (HSM) candidates that exhibit desirable characteristics like high porosity, crystallinity, large surface area, and an economical synthesis route.[5] Typically, MOFs consist of inorganic metal-oxide clusters bridged by organic linkers. For example, one of the first MOFs reported to exhibit H_2 sorption properties was isoreticular MOF (IRMOF-1), synthesized by Yaghi and coworkers, which consists of Zn_4O metal clusters linked together by 1,4-benzene dicarboxylate (BDC) units.[6] In practice, both the inorganic and organic building blocks could be chemically modified or even replaced, while keeping the highly porous framework structure intact. This offers extensive design flexibility and thus the potential for extensive optimization of the associated hydrogen storage capacity (for various examples, please see ref 5 and references therein).

Recent H_2 saturation uptake studies show that a family of IRMOFs could exhibit sorption capacities ranging from 2.0 to 7.5 wt % H_2 at 77 K with saturation pressures varying between 25 to 80 bar.[7] A recent computational study also suggested that the uptake characteristics of IRMOFs is closely related to the heat of adsorption, surface area, and free volume at low, moderate, and high pressures, respectively.[8] Their simple, theoretical estimates based on accessible surface area and free volume indicates that IRMOFs could potentially meet the U.S. Department of Energy (DOE)

* To whom correspondence should be addressed. E-mail: mhg@cchem.berkeley.edu.

(1) Fichtner, M. *Adv. Eng. Mater.* **2005**, *7*, 443–455.
(2) Schlapbach, L. *MRS Bull.* **2002**, *27*, 675.
(3) Zhou, L. *Renewable Sustainable Energy Rev.* **2005**, *9*, 395–408.
(4) Zuttel, A. *Naturwissenschaften* **2004**, *91*, 157–172.
(5) Rowsell, J. L. C.; Yaghi, O. M. *Angew. Chem., Int. Ed.* **2005**, *44*, 4670–4679.
(6) Rosi, N. L.; Eckert, J.; Eddaoudi, M.; Vodak, D. T.; Kim, J.; O'Keeffe, M.; Yaghi, O. M. *Science* **2003**, *300*, 1127–1129.
(7) Wong-Foy, A. G.; Matzger, A. J.; Yaghi, O. M. *J. Am. Chem. Soc.* **2006**, *128*, 3494–3495.
(8) Frost, H.; Duren, T.; Snurr, R. Q. *J. Phys. Chem. B* **2006**, *110*, 9565–9570.

10.1021/ic701625g CCC: $40.75
Published on Web 04/19/2008

gravimetric and volumetric targets for hydrogen storage.[9] However, for practical purposes, the H_2 sorption capacities at room temperature and moderate pressures are drastically reduced to less than 1 wt %.[8,10] This is because H_2 weakly physisorbed on these materials cannot survive at ambient conditions.

Both experiments[6,11,12] and various theoretical studies[13–16] suggest that the two main adsorptive sites for H_2 on the MOF are the metal oxide center and the organic linker unit. The strength of the interaction of H_2 with the latter is expected to be quite weak (about 4–5 kJ/mol) dominated by van der Waals interactions. The binding with the metal-oxide site is a little stronger (less than 10 kJ/mol) as this interaction could also be influenced by electrostatic and other orbital interactions. These weak binding affinities of H_2 are directly responsible for the low H_2 uptake characteristics exhibited by MOFs under ambient conditions. For reversible sorption and desorption of H_2 at room temperature and moderate pressures, the strength of the H_2 binding interaction should, ideally, be in the range of 20–40 kJ/mol.[13,17]

Therefore, a critical issue for the future practical application of MOFs for hydrogen storage is to devise strategies that enhance the H_2 binding affinity. In a recent computational study of simple model systems, we explored the range of attainable molecular hydrogen binding energies and demonstrated that the strength of the H_2 binding affinity is inextricably connected to the fundamental nature and mode of the H_2 interaction.[17] Molecular H_2 can interact with a host material through dispersive forces and also electrostatic and donor–acceptor type orbital interactions. Depending on the relative importance of these interactions, the H_2 binding energies could possibly vary between about 4 kJ/mol to above 300 kJ/mol without H_2 losing its molecular form! In particular, we found that unsaturated or partially charged metal centers had a tremendous effect on the binding affinity as electrostatic charge-quadrupole, charge-induced dipole effects and donor–acceptor interactions like forward and back-donation between H_2 and the metal complex could enhance the H_2 binding affinity. These factors could also be used as a tool to tune the strength of interaction to the ideal range by designing materials that promoted these type of effects.[17] For example, theoretical studies indicate that alkali-metal or transition metal coated fullerenes could be potential HSMs with relatively higher heats of adsorption.[18–21]

Incorporating or exposing open/unsaturated metal centers in the MOF is one strategy suggested to improve the H_2 interaction with the framework.[5] Typically in such MOFs, one of the ligands attached to the metal center is removed to expose open metal sites, without collapsing the framework. For example, MOF-505 is a Cu-based MOF with $Cu_2(CO_2)_4$ units in a paddle wheel structure linked by biphenyltetracarboxylate organic groups (BPTC), which was demonstrated to show about 2.5 wt % H_2 uptake at 77 K and 0.1 MPa.[22] A computational study based on this MOF revealed that the metal-oxide center was the preferred binding site with an adsorption energy that varied between 9 and 13 kJ/mol, depending upon the binding configuration of H_2.[10] Other experimentally observed examples of MOFs that display slightly higher heats of adsorption with unsaturated/open metal centers include Mg−MOF (~ 9.5 kJ/mol),[23] Prussian blue analogues (~7.4 kJ/mol),[24] MOF-74 (~8.3 kJ/mol),[25] and HKUST-1 (~6.6 kJ/mol).[26] An alternative strategy that has been adopted to incorporate open metal sites in the framework is to embed the metal within the organic linker.[27,28] Recently, a Co-based MOF (PCN-9) with entatic metal centers was reported to have an uptake of ~1.5 wt % H_2 at 77 K and 1 atm with the heat of adsorption measured to be about ~10.1 kJ/mol.[29] Although these examples show marginally improved adsorption energies, none of them are strong enough to survive under ambient conditions.

In this computational study, we explore another strategy where open transition metal sites could be incorporated over the organic linkers such as BDC, similar in spirit to the recently suggested theoretical design of organometallic bucky balls.[21] It is long known that molecular hydrogen can form stable "nonclassical" sigma-bonded complexes[30,31] with transition metals following the groundbreaking discovery of Kubas in the mid-1980s.[32] The coordination chemistry of molecular hydrogen with transition metals is thoroughly documented through decades of experimental[31,33–36] and

(9) Explanations of FreedomCAR/DOE hydrogen storage technical targets. http://www.eere.energy.gov./hydrogenandfuelcells/pdfs/freedomcar_target_explanations.pdf, Jan 2005.
(10) Yang, Q. Y.; Zhong, C. L. *J. Phys. Chem. B* **2006**, *110*, 655–658.
(11) Rowsell, J. L. C.; Eckert, J.; Yaghi, O. M. *J. Am. Chem. Soc.* **2005**, *127*, 14904–14910.
(12) Kubota, Y.; Takata, M.; Matsuda, R.; Kitaura, R.; Kitagawa, S.; Kato, K.; Sakata, M.; Kobayashi, T. C. *Angew. Chem., Int. Ed.* **2005**, *44*, 920–923.
(13) Garberoglio, G.; Skoulidas, A. I.; Johnson, J. K. *J. Phys. Chem. B* **2005**, *109*, 13094–13103.
(14) Sagara, T.; Klassen, J.; Ortony, J.; Ganz, E. *J. Chem. Phys.* **2005**, *123*, 014701.
(15) Yang, Q. Y.; Zhong, C. L. *J. Phys. Chem. B* **2005**, *109*, 11862–11864.
(16) Hamel, S.; Cote, M. *J. Chem. Phys.* **2004**, *121*, 12618–12625.
(17) Lochan, R. C.; Head-Gordon, M. *Phys. Chem. Chem. Phys.* **2006**, *8*, 1357–1370.
(18) Sun, Q.; Jena, P.; Wang, Q.; Marquez, M. *J. Am. Chem. Soc.* **2006**, *128*, 9741–9745.
(19) Yildirim, T.; Ciraci, S. *Phys. Rev. Lett.* **2005**, *94*, 175501.
(20) Yildirim, T.; Iniguez, J.; Ciraci, S. *Phys. Rev. B* **2005**, *72*, 153403.
(21) Zhao, Y. F.; Kim, Y. H.; Dillon, A. C.; Heben, M. J.; Zhang, S. B. *Phys. Rev. Lett.* **2005**, *94*, 155504.
(22) Chen, B. L.; Ockwig, N. W.; Millward, A. R.; Contreras, D. S.; Yaghi, O. M. *Angew. Chem., Int. Ed.* **2005**, *44*, 4745–4749.
(23) Dinca, M.; Long, J. R. *J. Am. Chem. Soc.* **2005**, *127*, 9376–9377.
(24) Kaye, S. S.; Long, J. R. *J. Am. Chem. Soc.* **2005**, *127*, 6506–6507.
(25) Rosi, N. L.; Kim, J.; Eddaoudi, M.; Chen, B. L.; O'Keeffe, M.; Yaghi, O. M. *J. Am. Chem. Soc.* **2005**, *127*, 1504–1518.
(26) Chui, S. S. Y.; Lo, S. M. F.; Charmant, J. P. H.; Orpen, A. G.; Williams, I. D. *Science* **1999**, *283*, 1148–1150.
(27) Kitaura, R.; Onoyama, G.; Sakamoto, H.; Matsuda, R.; Noro, S.; Kitagawa, S. *Angew. Chem., Int. Ed.* **2004**, *43*, 2684–2687.
(28) Kitagawa, S.; Noro, S.; Nakamura, T. *Chem. Commun.* **2006**, 701–707.
(29) Ma, S. Q.; Zhou, H. C. *J. Am. Chem. Soc.* **2006**, *128*, 11734–11735.
(30) Kubas, G. J. *Metal Dihydrogen and [Sigma]-bond Complexes: [Structure, Theory, and Reactivity]*; Kluwer Academic/Plenum Publishers: New York, 2001.
(31) Kubas, G. J. *Chem. Rev.* **2007**, *107*, 4152–4205.
(32) Kubas, G. J.; Ryan, R. R.; Swanson, B. I.; Vergamini, P. J.; Wasserman, H. J. *J. Am. Chem. Soc.* **1984**, *106*, 451–452.
(33) Maseras, F.; Lledos, A.; Clot, E.; Eisenstein, O. *Chem. Rev.* **2000**, *100*, 601–636.

theoretical research.[37–42] It is well-known that the magnitude of the transition metal−dihydrogen bond can vary between 20 and 160 kJ/mol depending on the nature of the metal core and the ligand environment.[30,31,33,43–45] These factors could be systematically and effectively used to tune the H_2 binding affinity and also enhance the magnitude of affinity by several folds compared to the strategies discussed in the previous paragraph.[31]

In particular, transition metals like Cr are known to form stable, half-sandwich complexes like (η^6-C_6H_6)$Cr(CO)_3$ (**1**). This complex has been studied extensively through both experiments[46–50] and theory.[51–55] There is experimental evidence to show that molecular hydrogen could coordinate with the metal core to form stable "nonclassical" sigma-bonded H_2 complexes[30] such as (η^6-C_6H_6)$Cr(CO)_2(H_2)$ (**2**) with the estimated $Cr-H_2$ bond dissociation energy being >17 kcal/mol (~70 kJ/mol).[56,57] It is also known that several arenes including ($C_6H_4(CO_2Me)_2$) (a BDC derivative) can coordinate with $Cr(CO)_3$ to form stable, piano-stool shaped η^6-complexes (for example, see refs 50, 58, and references therein). Therefore, it might be possible to synthesize hybrid MOFs where the $Cr(CO)_3$ groups are complexed to the organic linkers such as BDC. Subsequently, the CO ligands could be removed (either thermally or photolytically, and hopefully without collapsing the framework) to allow up to three H_2 molecules to interact with the resulting coordinatively unsaturated (η^6-BDC)$Cr(CO)_n$ (n = 0–2) complexes. A possible scheme is shown below:

$$(\eta^6\text{-BDC})Cr(CO)_3 \xrightarrow[n H_2]{\Delta \text{ or } h\nu} (\eta^6\text{-BDC})Cr(CO)_{3-n}(\eta^2\text{-}H_2)_n + n CO \quad (1)$$

Our experimental collaborators who are in the process of investigating the feasibility of this scheme originally envisioned this strategy.[59] In this study, with the help of computational tools like the density functional theory (DFT),[60] we hope to systematically assess and analyze the nature of the H_2 interaction with the resulting Cr−BDC complex, with the aim of providing useful information that would aid in optimizing the design of such hybrid materials.

In this investigation, we initially adopt the benzene analogue as a model of the potential H_2 binding site to study the nature of the binding configuration and also to estimate the strength of the metal−dihydrogen interaction. As mentioned earlier, the ligand environment and the nature of the metal core significantly influence the strength of the $M-H_2$ σ bond.[30,31,33,42,61] Therefore, we systematically analyze how factors like introducing π-donating and π- accepting arene-substituents (like $-CH_3$, $-NH_2$, $-OH$, $-OCH_3$, $-F$, $-Cl$, $-CF_3$) and changing the metal core (to V^-, Mn^+, and Mo) affect the $M-H_2$ binding interaction. Understanding these trends will help us to predict the control factors that are most likely to tune the H_2 interaction strength toward the ideal binding range. On the basis of the initial results, we also extend our analysis to the more realistic binding site models like the species shown in eq 1. In the last part of the paper, we apply energy decomposition analysis to break down the hydrogen binding energies into component parts. This enables us to take a detailed look at the factors controlling trends in the calculated binding affinities from another perspective.

II. Computational Methods. II.A Details of the Energy and Gradient Calculations. All reported calculations were performed with the QCHEM computational software.[62] DFT calculations were carried out using the exchange functional of Becke[63] and Perdew's correlation functional[64] (BP86). DFT is a powerful computational tool often used to study

(34) Crabtree, R. H. *Angew. Chem., Int. Ed. Eng.* **1993**, *32*, 789–805.
(35) Jessop, P. G.; Morris, R. H. *Coord. Chem. Rev.* **1992**, *121*, 155–284.
(36) McGrady, G. S.; Guilera, G. *Chem. Soc. Rev.* **2003**, *32*, 383–392.
(37) Andrews, L. *Chem. Soc. Rev.* **2004**, *33*, 123–132.
(38) Lin, Z. Y.; Hall, M. B. *Coord. Chem. Rev.* **1994**, *135*, 845–879.
(39) Heinekey, D. M.; Lledos, A.; Lluch, J. M. *Chem. Soc. Rev.* **2004**, *33*, 175–182.
(40) *Transition Metal Hydrides*; Dedieu, A., Ed.; VCH Publishers, Inc.: New York, 1992.
(41) Musaev, D. G.; Morokuma, K. *Adv. Chem. Phys.* **1996**, *95*, 61–128; Vol. 95, Surface Properties.
(42) Frenking, G.; Frohlich, N. *Chem. Rev.* **2000**, *100*, 717–774.
(43) Coe, B. J.; Glenwright, S. J. *Coord. Chem. Rev.* **2000**, *203*, 5–80.
(44) Ehlers, A. W.; Dapprich, S.; Vyboishchikov, S. F.; Frenking, G. *Organometallics* **1996**, *15*, 105–117.
(45) Gagliardi, L.; Pyykko, P. *J. Am. Chem. Soc.* **2004**, *126*, 15014–15015.
(46) Rees, B.; Coppens, P. *Acta Crystallogr., Sect. B: Struct. Sci.* **1973**, *B 29*, 2516–2528.
(47) Sickafoose, S. M.; Breckenridge, S. M.; Kukolich, S. G. *Inorg. Chem.* **1994**, *33*, 5176–5179.
(48) Kukolich, S. G.; Sickafoose, S. M.; Flores, L. D.; Breckenridge, S. M. *J. Chem. Phys.* **1994**, *100*, 6125–6128.
(49) Kukolich, S. G. *J. Am. Chem. Soc.* **1995**, *117*, 5512–5514.
(50) Hunter, A. D.; Shilliday, L.; Furey, W. S.; Zaworotko, M. J. *Organometallics* **1992**, *11*, 1550–1560.
(51) Suresh, C. H.; Koga, N.; Gadre, S. R. *Organometallics* **2000**, *19*, 3008–3015.
(52) Low, A. A.; Hall, M. B. *Int. J. Quantum Chem.* **2000**, *77*, 152–160.
(53) Schleyer, P. V.; Kiran, B.; Simion, D. V.; Sorensen, T. S. *J. Am. Chem. Soc.* **2000**, *122*, 510–513.
(54) Simion, D. V.; Sorensen, T. S. *J. Am. Chem. Soc.* **1996**, *118*, 7345–7352.
(55) Li, Y.; McGrady, J. E.; Baer, T. *J. Am. Chem. Soc.* **2002**, *124*, 4487–4494.
(56) Walsh, E. F.; George, M. W.; Goff, S.; Nikiforov, S. M.; Popov, V. K.; Sun, X. Z.; Poliakoff, M. *J. Phys. Chem.* **1996**, *100*, 19425–19429.
(57) Goff, S. E. J.; Nolan, T. F.; George, M. W.; Poliakoff, M. *Organometallics* **1998**, *17*, 2730–2737.
(58) Hunter, A. D.; Mozol, V.; Tsai, S. D. *Organometallics* **1992**, *11*, 2251–2262.
(59) Kaye, S. S.; Dinca, M.; Long, J. R. Private communication, 2006.
(60) Parr, R. G.; Yang, W. *Density-functional theory of atoms and molecules*; Oxford: New York, 1989.
(61) Nemcsok, D. S.; Kovacs, A.; Rayon, V. M.; Frenking, G. *Organometallics* **2002**, *21*, 5803–5809.
(62) Shao, Y.; Molnar, L. F.; Jung, Y.; Kussmann, J.; Ochsenfeld, C.; Brown, S. T.; Gilbert, A. T. B.; Slipchenko, L. V.; Levchenko, S. V.; O'Neill, D. P.; DiStasio, R. A.; Lochan, R. C.; Wang, T.; Beran, G. J. O.; Besley, N. A.; Herbert, J. M.; Lin, C. Y.; Van Voorhis, T.; Chien, S. H.; Sodt, A.; Steele, R. P.; Rassolov, V. A.; Maslen, P. E.; Korambath, P. P.; Adamson, R. D.; Austin, B.; Baker, J.; Byrd, E. F. C.; Dachsel, H.; Doerksen, R. J.; Dreuw, A.; Dunietz, B. D.; Dutoi, A. D.; Furlani, T. R.; Gwaltney, S. R.; Heyden, A.; Hirata, S.; Hsu, C. P.; Kedziora, G.; Khalliulin, R. Z.; Klunzinger, P.; Lee, A. M.; Lee, M. S.; Liang, W.; Lotan, I.; Nair, N.; Peters, B.; Proynov, E. I.; Pieniazek, P. A.; Rhee, Y. M.; Ritchie, J.; Rosta, E.; Sherrill, C. D.; Simmonett, A. C.; Subotnik, J. E.; Woodcock, H. L.; Zhang, W.; Bell, A. T.; Chakraborty, A. K.; Chipman, D. M.; Keil, F. J.; Warshel, A.; Hehre, W. J.; Schaefer, H. F.; Kong, J.; Krylov, A. I.; Gill, P. M. W.; Head-Gordon, M. *Phys. Chem. Chem. Phys.* **2006**, *8*, 3172–3191.
(63) Becke, A. D. *Phys. Rev. A* **1988**, *38*, 3098–3100.
(64) Perdew, J. P. *Phys. Rev. B* **1986**, *33*, 8822–8824.

organometallic chemistry.[65,66] In particular, BP86 is a quite widely used density functional with a good performance to cost ratio, that is known for its consistent and reliable prediction of geometry, vibrational frequencies, and bond energies of transition metal complexes.[67–74] BP86 has also been successfully applied to study Group VI transition metal dihydrogen sigma complexes.[30,61,75] A triple split valence Pople-type basis with a set of d- and f-type polarization functions on the heavy atoms and a set of p- and d-functions on the hydrogen atoms (6–311G**) was employed.[76,77] The small core (Ne) Stuttgart-Born (SRSC) effective core potential (ECP) was used to describe the core–electrons of all the transition metals considered in this study.[78,79] The integrals were evaluated on a large quadrature grid of size (99,590) (i.e., 99 radial points and 590 angular points per radial point). The use of triple-ζ quality basis with additional polarization functions, small core ECP, and large grid size satisfy previous recommendations for obtaining reliable results using DFT with functionals like BP86.[68,80]

In a recent separate investigation,[81] we studied the performance of density functionals, BP86 and B3LYP[82] (with 6–311G** basis and SRSC core potential) in predicting the structural features and bond dissociation energies of a set of Group VI transition metal complexes that can be closely associated with the systems considered in the current study. We found that BP86 consistently predicted better structures and bond energies than B3LYP.[81] The results were compared not only against available experimental data, but also with the predictions of the sophisticated coupled cluster singles and doubles with perturbative triples correction (CCSD(T)) method.[83] On the basis of the conclusions of this study,[81] we choose to optimize and treat all the transition metal complexes studied in this paper at the BP86/SRSC/6–311G** level of theory. Different initial configurations were employed to explore the potential energy surface. Only lowest energy configurations that were verified to be valid local minima with no imaginary frequencies are reported.

The average $M-H_2$ bond dissociation energies for the various complexes considered are evaluated as follows:

$$D_e = (E_{Complex} + nE_{H_2} - E_{Complex-(H_2)_n})/n \qquad (2)$$

We report both the electronic dissociation energy (D_e) and the zero-point vibrational energy corrected D_0. Furthermore, vibrational analysis indicated that the thermodynamic corrections arising from finite temperature effects due to the changes in the translational, rotational, and vibrational degrees of freedom, as well as pV work (assuming ideal behavior), are about 6–7 kJ/mol or lower per H_2 molecule for all the complexes considered in this study. So the calculated average dissociation energies D_0. could be up to 6–7 kJ/mol higher at 298 K. The reported electronic D_e is *not* corrected for basis set superposition effects (BSSE) based on previous recommendations.[84] Moreover, we found that the BSSE correction estimated for a few representative complexes at the BP86/SRSC/6–311G** level to be less than 3 kJ/mol per H_2 molecule and therefore choose to ignore this error.[80]

II.B Analysis of Donor–Acceptor Interactions in Transition Metal$-H_2$ Complexes. Sigma-bonded $TM-H_2$ complexes are greatly influenced by donor–acceptor interactions like forward donation of σ H−H electrons to the empty metal orbitals and back-donation from the metal into the antibonding σ^* H_2 orbitals.[30,44] These effects are directly responsible for any elongation observed in the H−H bond length. We therefore use trends in the H−H bond length and $M-H_2$ distance (measured from the metal center to the center-of-mass of the H_2 molecule) in the optimized complex structures as probes to understand the mode of the $M-H_2$ interaction. Since donor–acceptor interactions are generally the strongest $TM-H_2$ coupling, we could also expect changes in bond distances to be strongly correlated with trends observed in the binding affinity. We adopt this straightforward approach to understanding observed changes in the $TM-H_2$ interactions in section III of the paper because of its simplicity and because it is based only on inferences from experimental observables (structure and binding energy).

However, this may well be an oversimplified view, since $TM-H_2$ interactions are in reality the net result of a set of large and partially canceling energy changes. We therefore further examine the detailed origin of the H_2 interaction with the host medium in section IV by decomposing the estimated electronic dissociation energy into physically relevant components such as the contribution from interacting "frozen monomer densities" (FRZ), the energy lowering due to polarization (POL) of the densities (without charge transfer), and the further energy lowering due to charge transfer (CT)

(65) Ziegler, T. *Pure Appl. Chem.* **1991**, *63*, 873–878.
(66) Ziegler, T. *Chem. Rev.* **1991**, *91*, 651–667.
(67) Frenking, G.; Wagener, T. Transition Metal Chemistry. In *Encyclopedia of Computational Chemistry*; Wiley: New York, 1998.
(68) Torrent, M.; Sola, M.; Frenking, G. *Chem. Rev.* **2000**, *100*, 439–493.
(69) Furche, F.; Perdew, J. P. *J. Chem. Phys.* **2006**, *124*, 044103.
(70) Hyla-Kryspin, I.; Grimme, S. *Organometallics* **2004**, *23*, 5581–5592.
(71) Buhl, M.; Kabrede, H. *J. Chem. Theory Comput.* **2006**, *2*, 1282–1290.
(72) Gonzalez-Blanco, O.; Branchadell, V. *J. Chem. Phys.* **1999**, *110*, 778–783.
(73) Jonas, V.; Thiel, W. *J. Chem. Phys.* **1996**, *105*, 3636–3648.
(74) Szilagyi, R. K.; Frenking, G. *Organometallics* **1997**, *16*, 4807–4815.
(75) Li, J.; Ziegler, T. *Organometallics* **1996**, *15*, 3844–3849.
(76) Krishnan, R.; Binkley, J. S.; Seeger, R.; Pople, J. a. *J. Chem. Phys.* **1980**, *72*, 650–654.
(77) Mclean, A. D.; Chandler, G. S. *J. Chem. Phys.* **1980**, *72*, 5639–5648.
(78) Dolg, M.; Wedig, U.; Stoll, H.; Preuss, H. *J. Chem. Phys.* **1987**, *86*, 2123–2131.
(79) Andrae, D.; Haussermann, U.; Dolg, M.; Stoll, H.; Preuss, H. *Theor. Chim. Acta* **1990**, *77*, 123–141.
(80) Rosa, A.; Ehlers, A. W.; Baerends, E. J.; Snijders, J. G.; Velde, G. T. *J. Phys. Chem.* **1996**, *100*, 5690–5696.
(81) Lochan, R. C.; Shao, Y. H.; Head-Gordon, M. *J. Chem. Theory Comput.* **2007**, *3*, 988–1003.
(82) Becke, A. D. *J. Chem. Phys.* **1993**, *98*, 1372–1377.
(83) Raghavachari, K.; Trucks, G. W.; Pople, J. A.; Head-Gordon, M. *Chem. Phys. Lett.* **1989**, *157*, 479–483.
(84) Frenking, G.; Antes, I.; Böhme, M.; Dapprich, S.; Ehlers, A. W.; Jonas, V.; Neuhaus, A.; Otto, M.; Stegmann, R.; Veldkamp, A.; Vyboishchikov, S. F. Pseudopotential Calculations of Transition Metal Compunds: Scope and Limitations. In *Reviews in Computational Chemistry*; Lipkowitz, K. B., Boyd, D. B., Eds.; VCH Publishers, Inc.: New York, 1996; Vol. *8*.

effects like forward donation (FD) by the H_2 bonding pair of electrons to the metal ($H_2 \rightarrow$ M FD) and metal back-donation (BD) to the antibonding σ^* orbitals of H_2 (M $\rightarrow$ H_2 BD). This is accomplished using our recently introduced energy decomposition analysis (EDA) scheme.[85] It is important to state clearly that there is no uniquely "best" EDA, and different methods can (and will) produce somewhat different results. The method we employ is similar conceptually to existing EDA methods such as the Morokuma analysis and others[42,86] but includes two important new features. First is a fully self-consistent treatment of the energy lowering due to polarization, which is evaluated by a self-consistent field calculation in which the molecular orbital coefficient is constrained to be block-diagonal in the interacting fragments to prohibit charge transfer. This results in MOs that are absolutely localized on the fragments (ALMOs),[87] and the constrained SCF is often called SCF for molecular interactions (SCF-MI).[88–90] The second new feature is the ability to separate forward and back-donation in the charge transfer term using a perturbative single Roothaan step approximation starting from the SCF-MI reference.[85,91] Because the single Roothaan step does not exactly describe the energy lowering associated with relaxing the SCF-MI solution to the full SCF solution, there is also an additional (generally small) "higher order relaxation" energy (ΔE_{CT}^{HO}) associated with this part of the decomposition. This is specified in the relevant tables given in section IV and is of the order of 3–8 kJ/mol per H_2 molecule for all systems considered in this study.

In this EDA based on ALMOs, the average H_2 binding energy ΔE^* ($= -D_e^*$) is defined as follows:

$$\Delta E^* = -D_e^* = (E_{\text{Complex}-(H_2)_n} - E_{\text{Complex}^*} - nE_{H_2}^*)/n \quad (3)$$

Here, $E_{\text{Complex}-H_2}$ represents the total SCF energy obtained at the BP86/SRSC/6–311G** optimized geometry of the complex, while E_{Complex^*} and $E_{H_2}^*$ are the SCF energies of the infinitely separated fragments fixed at the geometry of the complex. The energy required to distort the free, relaxed fragments to the final complex geometry is called the "geometry distortion" (GD) term:

$$D_e = D_e^* + E_{GD} \quad (4)$$

Using ALMOs and SCF MI, the ΔE^* can be decomposed into

$$\Delta E^* = \Delta E_{FRZ} + \Delta E_{POL} + \Delta E_{CT} \quad (5)$$

Here, the ΔE_{FRZ} term represents the combined effects of the Coulomb repulsion and the exchange-correlation contribution of the DFT functional used, while ΔE_{POL} and ΔE_{CT} represent the polarization and charge transfer components of the total interaction energy, respectively. By using the single Roothaan step perturbative treatment, the ΔE_{CT} can be further decomposed into the bonding and back-bonding contributions and generally small MO relaxation term:[85]

$$\Delta E_{CT} = -\Delta E_{H_2 \rightarrow \text{M FD}} + \Delta E_{\text{M} \rightarrow H_2 \text{ BD}} + \Delta E_{CT}^{HO} \quad (6)$$

Note that as a result of using DFT, we do not account for the dispersive component of the interaction energy. However, as donor–acceptor interactions are likely to play the dominant role in the systems of interest, we expect the dispersive contributions to be relatively very small compared to the effects defined above.

Figure 1. Color code used for the atoms in all figures.

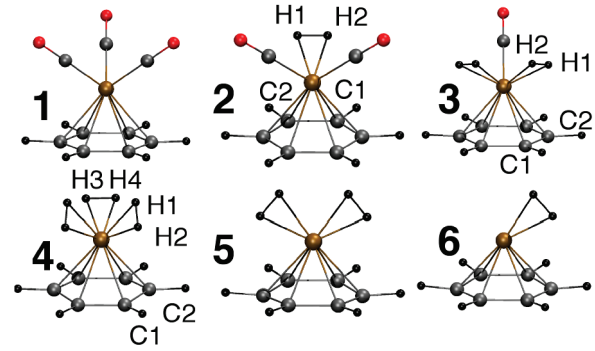

Figure 2. Optimized structures of $(C_6H_6)Cr(CO)_{3-n}(H_2)_n$ (n = 0–3; **1**–**4**) and $(C_6H_6)Cr(H_2)_n$ (n = 1, 2; **5**–**6**) complexes.

III. Results and Discussion

In this section, we report and discuss the important structural features of the optimized geometries. In particular, these key features include the M−H_2 and M−Arene bond distances (measured from the metal to the center-of-mass of the H−H bond or the centroid of the arene plane, respectively), the H−H, C−O, and M−CO bond lengths, and the trends observed in the calculated M−H_2 bond dissociation energies for the various complexes considered. Figure 1 indicates the color coding scheme used in all the figures.

III.A Effect of CO Ligands. The optimized structures of the species $(C_6H_6)Cr(CO)_{3-n}(H_2)_n$ (n = 0–3; named **1**, **2**, **3**, and **4**, respectively) are shown in Figure 2, and the important bond distances obtained are tabulated in Table 1. The parent half-sandwich $(C_6H_6)Cr(CO)_3$ molecule (**1**) exhibits a staggered D_{3v} symmetry with structural features that are very close to the experimental values.[46–49] In **2**, **3**, and **4**, the H_2 molecules bind associatively to form sigma-type complexes with the metal center. The H−H bond axis in **2** is parallel to the arene plane (Bond angles, H1−H2−C2 = C1−C2−H2 = 66.2° and adjacent angles H1−H2−C1 (96°) and H2−C1−C2 (84°) are supplementary, see Figure 2), while in **3** it rotates a little bit to have bond angles H1−H2−C2 = 53.9° and C1−C2−H2 = 67.1°. The lowest energy configuration corresponding to complex **4** was found to have one of the H_2 molecules (H3−H4 in Figure 2) parallel to the arene ring (similar to **2**) while the remaining two H_2

(85) Khaliullin, R. Z.; Cobar, E. A.; Lochan, R. C.; Head-Gordon, M.; Bell, A. T. *J. Phys. Chem. A* **2007**, *111*, 8753–8765.
(86) Morokuma, K. *J. Chem. Phys.* **1971**, *55*, 1236.
(87) Stoll, H.; Wagenblast, G.; Preuss, H. *Theor. Chim. Acta* **1980**, *57*, 169–178.
(88) Khaliullin, R. Z.; Head-Gordon, M.; Bell, A. T. *J. Chem. Phys.* **2006**, *124*, 204105.
(89) Nagata, T.; Takahashi, O.; Saito, K.; Iwata, S. *J. Chem. Phys.* **2001**, *115*, 3553–3560.
(90) Gianinetti, E.; Vandoni, I.; Famulari, A.; Raimondi, M. *Adv. Quantum Chem.* **1998**, *31*, 251.
(91) Liang, W. Z.; Head-Gordon, M. *J. Phys. Chem. A* **2004**, *108*, 3206–3210.

Table 1. Effect of CO ligands: Structural Features (in pm) and Calculated Cr−H_2 Bond Dissociation Energies Per H_2 Molecule (in kJ/mol) for the $(C_6H_6)Cr(CO)_{3-n}(H_2)_2$ (n = 1–3) Complexes

system	Cr−CO	Cr−Arene	C−O	Cr−H_2	H−H	D_e	D_0
			113.9[a]		75.2[a]		
1 $(C_6H_6)Cr(CO)_3$	183.9	171.8	116.7				
2 $(C_6H_6)Cr(CO)_2(H_2)$	183.4	169.2	117.0	163.2	87.2	96.9	77.2
3 $(C_6H_6)Cr(CO)_2(H_2)_2$	183.0	166.9	117.3	162.5	88.3	88.6	71.6
4 $(C_6H_6)Cr(H_2)_3$		163.8		162.0[b]	89.5[b]	85.5	68.4
				162.6[c]	88.2[c]		

[a] Free C−O and H−H bond length (BP86/6–311G**). [b] Distance corresponding to H1−H2 (see Figure 2). [c] Distance corresponding to H3−H4 (see Figure 2).

molecules appear to take up positions similar to **3**; however, the bond angle H1−H2−C2 (in Figure 2) is now increased to 105.3°, while C1−C2−H2 = 67.8°. The T_d type configuration where all three H_2 molecules lie symmetrically about the metal center, with their respective bond axes parallel to the arene, was found to be an invalid local minimum (with three imaginary frequencies), almost 12 kJ/mol higher in energy relative to **4**.

Table 1 indicates that as the number of CO ligands present in the parent complex **1** is decreased, the Cr−CO and Cr−Arene (distance between Cr and the center of the benzene ring) bond distances decrease by about 0.5 pm and 2–3 pm, respectively, while the C−O bond length increases by about 0.3 pm. This suggests that as good π-acceptor CO ligands are removed and replaced by the poor π-acceptor H_2 molecules, the metal core is able to relatively increase its back-donating ability to both arene and the remaining CO ligands, which in turn marginally increases the Cr−CO bond strength and hence elongates the C−O bond. A similar effect is observed experimentally with a red shift of the C−O vibrational frequency when one of the ligands in **1** is replaced with a less π-acidic triphenylphosphine ligand.[92] However, the H−H bond distances appear to be considerably elongated (almost 12–14 pm) from the free "H−H" bond length estimated at the same level of theory (∼75 pm) and increases as we move from complex **2** to **4**. This again suggests that the metal to H_2 back-donation is significant and increases as the number of CO ligands is decreased.[61,93] We would therefore expect the Cr−H_2 interaction energy and bond distance to decrease from **2** to **4**.

The average Cr−H_2 bond dissociation energies obtained per H_2 molecule for the complexes **2**, **3**, and **4** are summarized in Table 1. The electronic dissociation energies (D_e) range between 86 and 96 kJ/mol. The zero-point energy corrections to the D_e value appear to be on the order of −17 to −20 kJ/mol. The calculated D_0 value for the complex **2** of ∼77 kJ/mol is consistent with the estimates from the time-resolved infrared absorption spectroscopy experimental study (>17−71 kJ/mol).[94] The estimated D_0 value decreases by ∼ 9 kJ/mol when we move from complex **2** to **4**. Although the magnitude of change is quite small, we do not observe the trend expected from the above analysis of the H−H and Cr−H_2 bond distances. This is probably because the D_0 represents the "average" H_2 bond dissociation energy. For instance, if we consider the incremental bond dissociation energies evaluated as,

Table 2. Structural Features (in pm) and Calculated Incremental Cr−H_2 Bond Dissociation Energies (see eq 2; in kJ/mol) for the $(C_6H_6)Cr(H_2)_n$ (n = 1–3) Complexes

system	Cr−Arene	Cr−H_2	H−H	D_e^{inc}	D_e^{inc}
			75.2[a]		
4 $(C_6H_6)Cr(H_2)_3$	163.8	162.0[b]	89.5[b]	81.1	63.0
		162.6[c]	88.2[c]		
5 $(C_6H_6)Cr(H_2)_2$	157.6	166.8	86.8	83.6	65.9
6 $(C_6H_6)Cr(H_2)$	153.1	163.5	90.6	91.7	76.3

[a] Free H−H bond length (BP86/6–311G**). [b] Distance corresponding to H1−H2 (see Figure 2). [c] Distance corresponding to H3−H4 (see Figure 2).

$$D_e^{inc} = E_{Complex-(H_2)_n} - E_{Complex-(H_2)_{n-1}} - nE_{H_2} \qquad (7)$$

for the complex **4** (see Table 2), we notice that the D_0^{inc} increases from ∼ 63 kJ/mol for **4** to ∼ 76 kJ/mol for the complex **6**, $(C_6H_6)Cr(H_2)$. Although the interaction of the first H_2 molecule with the species $(C_6H_6)Cr$ is as strong as the complex **2**, the magnitude of the H_2 binding affinity decreases by about 5–13% when subsequent H_2 molecules are introduced, which in turn reduces the average D_0 value to ∼68 kJ/mol. This trend indicates that the metal back-donation to the antibonding σ^* H_2 orbitals decreases marginally as the number of H_2 molecules clustered about the metal center increases.

In the context of H_2 storage, the observed H_2 binding affinities for the complexes **2**, **3**, and **4** appear to be too strong for easy desorption at ambient conditions (ideal binding energy range ∼20–40 kJ/mol). However, the higher binding energies do indicate that it should be possible to achieve higher sorption capacities at room temperature for these hybrid MOFs. To further understand the nature and characteristics of the H_2 interaction with the transition-metal species, we will look at the possible factors that might influence the H_2 binding affinity, which could likely help us to "tune" the strength of the H_2 interaction toward the ideal binding energy range.

III.B Effect of Arene Substituents. Hunter et al. have conducted systematic experimental studies on arene substituent effects on complex **1**.[50,58] π-donating arene substituents caused the M−Arene distance to decrease relative to complex **1** while the C−O vibrational frequency red-shifted, indicating increased back-donation to the CO and arene ligands and/or less forward donation. The reverse trend was observed with π-acidic substituents. This suggests that arene substitutents could also affect the H_2 binding affinity as their electronic effects could be transmitted through the metal

(92) Bitterwolf, T. E. *Polyhedron* **1988**, *7*, 1377–1382.
(93) Banister, J.a.; Lee, P. D.; Poliakoff, M. *Organometallics* **1995**, *14*, 3876–3885.
(94) Zheng, Y. F.; Wang, W. H.; Lin, J. G.; She, Y. B.; Fu, K. J. *J. Phys. Chem.* **1992**, *96*, 9821–9827.

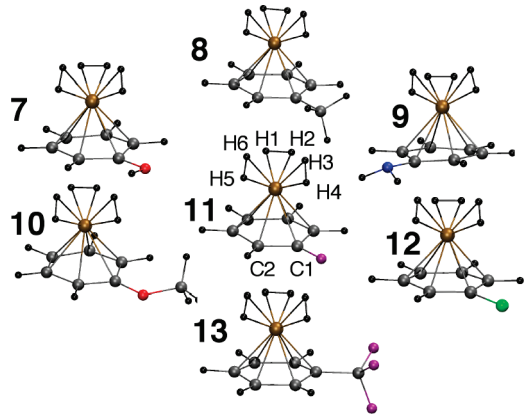

Figure 3. Optimized structures of $(X-C6H_5)Cr(H_2)_3$ (**7**–**13**) complexes.

Table 3. Effect of Substituents: Structural Features (in pm) and Calculated Average Cr−H_2 Bond Dissociation Energies Per H_2 Molecule (in kJ/mol) for the $(X-C_6H_5)Cr(H_2)_3$ (X = $-CH_3$, $-NH_2$, $-OH$, $-OCH_3$, $-F$, $-Cl$, $-CF_3$) Complexes

X	Cr−Arene	Cr−H_2[a]	H−H[a]	D_e	D_0
			75.2[b]		
4 H	163.8	162.0	89.5	85.5	68.4
		162.6	88.2		
7 OH	165.3	160.3	91.2	90.7	73.1
		162.0	88.4		
		162.7	87.8		
8 CH_3	164.2	161.6	89.9	86.6	69.6
		162.2	88.2		
		162.7	88.0		
9 NH_2	166.2	159.9	92.1	89.8	72.6
		162.3	88.1		
		162.4	88.1		
10 OCH_3	165.8	160.4	91.4	90.7	73.5
		161.6	88.9		
		162.6	87.9		
11 F	163.8	161.3	90.1	87.5	70.3
		162.3	88.0		
		163.4	87.2		
12 Cl	163.3	162.3	89.2	82.4	65.4
		163.2	87.2		
		163.6	87.1		
13 CF_3	163.1	162.5	88.7	83.4	66.1
		163.1	87.4		
		163.3	87.4		

[a] Multiple entries refer to H1−H2, H3−H4, and H5−H6 molecules, respectively (see Figure 3). [b] Free H−H bond length (BP86/6–311G**).

center to influence the M−H_2 interaction. We therefore investigated arene-substituent effects by introducing common functional groups like $-CH_3$, $-NH_2$, $-OH$, $-OCH_3$, $-F$, $-Cl$, $-CF_3$ on the benzene ring in the complex **4**. Figure 3 shows the lowest energy configurations obtained for the resulting $(X-C_6H_5)Cr(H_2)_3$ complexes (labeled **7**−**13**). The arene ring appears slightly distorted, especially at the site of the substituent, consistent with the observations of Hunter et al.[50,58] The H_2 molecules appear in the same form as the parent complex **4** with modest fluctuations in the Cr−Arene, Cr−H_2, and H−H bond distances, which suggests that the substituent effect is likely to be quite small. Nevertheless, it is interesting to study the resulting trends and analyze the extent of the substituent effect on the Cr−H_2 bond dissociation energies, as this may permit fine-tuning of these energies.

Table 3 summarizes the important bond distances obtained for these substituted complexes. π-donating substituents like $-CH_3$ (**8**), $-OH$(**7**), $-OCH_3$ (**10**), $-NH_2$ (**9**) increase the Cr−Arene distance by about 0.4–2 pm relative to complex **4** while the strong electron withdrawing groups like $-Cl$ (**12**) and $-CF_3$ (**13**) decrease the C−Arene distance by about 0.6 pm. The three bound H_2 molecules are influenced to different extents depending on their binding configuration. The H1−H2 molecule that lies almost parallel to the arene ring aligns itself along the C−C bond that lies across from the C1−C2 bond to which the substituent X is attached for π-donating substituents (see Figure 3), while another H_2 (H3−H4) lies almost above the substituent, leading to a distorted 'syn-eclipsed' conformation that was observed with complex **1** analogues.[50,58,95–97] In the strong π-accepting $-CF_3$ (**13**) complex, both H1−H2 and H3−H4 try to maximize their distance from the substituent, giving a distorted staggered conformation, again similar to complexes of **1**.[50,58] The Cr−(H1−H2) distances decreased for π-donating substituents (**7**, **8**, **9**, **10**, **11**) and the H1−H2 bond increases, indicating this Cr−H_2 interaction is marginally increased. The opposite trend is observed with the strong electron withdrawing groups **12** and **13**. There appears to be no specific trend associated with H3−H4. The interaction of the third H_2 molecule (H5−H6) with the Cr metal center appears to be weakened (longer Cr−H_2 and shorter H5−H6 distances) irrespective of the nature of the substituent. Overall, strong electron-withdrawing groups like $-Cl$ or $-CF_3$(which is also a good π-acceptor) generally weaken Cr−H_2 interactions in the complex.

The estimated D_e and D_0 values in Table 3 indicate that all π-donating substituents like complexes **7**–**10** slightly strengthen the H_2 binding interaction with the metal center relative to the parent complex **4** by 2–7%. The π-accepting $-CF_3$ group (**13**) decreases the dissociation enthalpy by about 3% while $-Cl$ (**12**) reduces it by about 4%. This trend is consistent with the structural changes and suggests that π-accepting ligands decrease the π-electron density of the ring, causing the metal to increase its back-donation to the arene, thereby strengthening its interaction with the ring and decreasing the Cr−Arene distance. This translates into reduced back-donation into the H−H σ^* antibonding orbitals, shortening the H−H bond and weakening the Cr−H_2 binding affinity. For $-F$ and $-Cl$, which could be reasonable π-donors but can also inductively withdraw electron-density, H_2 binding can increase or decrease depending upon which effect predominates.

Table 4 illustrates the effect of introducing substitutents like $-CF_3$ and $-Cl$ in the complexes of type **2** and **3** which have two and one CO ligands, respectively. The corresponding optimized geometries of complexes **14**−**17** are shown in Figure 4. Similar to the above discussion, the H_2 appear to maximize their distance from the $-CF_3$ group leading to a distorted staggered conformation in complexes **14** and **16** while in **13** and **15**, the ligands prefer a distorted syn-eclipsed type conformation with one of the H_2 molecules lying almost

(95) Albright, T.a.; Hofmann, P.; Hoffmann, R. *J. Am. Chem. Soc.* **1977**, *99*, 7546–7557.
(96) Chinn, J. W.; Hall, M. B. *J. Am. Chem. Soc.* **1983**, *105*, 4930–4941.
(97) Semmelhack, M. F.; Garcia, J. L.; Cortes, D.; Farina, R.; Hong, R.; Carpenter, B. K. *Organometallics* **1983**, *2*, 467–469.

Table 4. Effect of Substituents: Structural Features (in pm) and Calculated Average Cr−H_2 Bond Dissociation Energies Per H_2 Molecule (in kJ/mol) for the (X−C_6H_5)Cr(CO)$_{3-n}$(H_2)$_n$ (n = 1, 2; X = −H, −CF_3, −Cl) Complexes

X	Cr−CO	Cr−Arene	C−O	Cr−H_2	H−H	D_e	D_0	ΔH_{dis}
			113.9[a]		75.2[a]			
(X−C_6H_5)Cr(CO)$_2$(H_2)								
2 H	183.4	169.2	117.0	163.2	87.2	96.9	77.2	82.4
14 CF_3	184.9	168.4	117.0	166.6	85.5	91.7	73.9	77.2
15 Cl	183.6	169.0	116.9	164.3	86.1	91.6	74.1	77.4
(X−C_6H_5)Cr(CO)(H_2)$_2$								
3 H	183.0	166.9	117.3	162.5	88.3	88.6	71.6	78.0
16 CF_3	183.9	166.2	116.9	163.0	87.6	84.0	67.1	73.5
17 Cl	183.3	166.6	117.2	163.4[b]	87.1[b]	85.5	68.5	75.0
				162.9[c]	87.6[c]			

[a] Free C−O and H−H bond length (BP86/6–311G**). [b] Distance corresponding to H1−H2 (analogous to representation in Figure 2). [c] Distance corresponding to H3−H4 (analogous to representation in Figure 2).

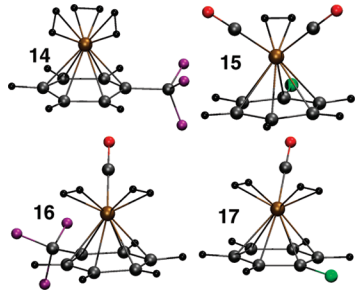

Figure 4. Optimized structures of (X−C_6H_5)Cr(CO)$_{2-n}$(H_2)$_n$ (n = 1, 2; X = CF_3, Cl; **14**–**17**) complexes.

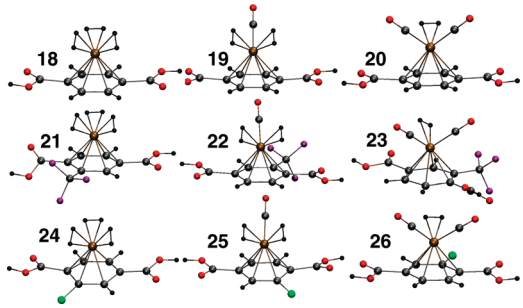

Figure 5. Optimized structures of (X−BDC)Cr(CO)$_{3-n}$(H_2)$_n$ (n = 1–3; X = H, CF_3, Cl; **18**–**26**) complexes.

above the −Cl. Shifts in distances relative to the parent complexes **2** and **3** indicate that the metal interaction with the arene is increased, thus indirectly weakening the Cr−CO and Cr−H_2 interactions. The computed D_0 values support this conclusion, with −CF_3 in the complexes **14** and **16** leading to a 4–6% decrease in the Cr−H_2 D_0 value relative to complex **2** and **3** while the −Cl group achieves about 4% reduction.

III.C Effect of Benzene Dicarboxylic Acid Substituents. Although the reduction in H_2 binding strength association with the π-accepting −CF_3 substituent discussed above is small (∼4 kJ/mol), one might consider employing multiple substituents to increase the effect. In the actual organic linker, BDC, there are two −COOH groups that are powerful electron-withdrawing groups, so we expect that the H_2 interaction would be further decreased in these cases. Therefore, we next examine the effect of substituents like −CF_3 and −Cl on the (BDC)Cr(CO)$_{3-n}$(H_2)$_n$ complex.

Figure 5 shows the optimized lowest energy configurations obtained for the BDC analogues of the complexes **2**−**4**. The H_2 molecules in complexes **18**−**20** appear to cluster around the Cr metal center in a distorted staggered conformation similar to their respective precursor complexes so that the ligands (both CO and H_2) are away from the −COOH groups.[50,58,95,98] The −CF_3 and −Cl analogues (**20**−**26**) also exhibit similar characteristics. The −COOH and −CF_3 groups are bent toward the Cr(CO)$_{3-n}$(H_2)$_n$ group while the −Cl group is bent away, which is consistent with the observations of Hunter et al.[50,58] Also in complexes **21** and **23**, the −COOH group closest to the substituent −CF_3 is significantly distorted out the arene plane. Table 5 lists the important bond distances measured from the optimized geometries of these BDC complexes. There are modest shifts (<1.5 pm) in the Cr−Arene distance, which are decreased relative to the respective benzene analogues except for complexes **18** and **24**, where the Cr−Arene separation increases by 0.2–0.5 pm, because of increased back-donation. Conversely in the CO containing complexes (**19**, **22, 25**, **20**, **23**, **26**), the Cr−CO distances increase by about 1 pm while the C−O bond length shrinks by about 0.4–0.5 pm with respect to the corresponding benzene precursors. The Cr−H_2 distance is increased by almost 2–3 pm in the −CF_3 complexes **21**−**23** relative to the complexes **4**, **3**, and **2** while the corresponding H−H bond lengths decrease by the same amount. Similar results are observed with the −Cl complexes **24**−**26**. This suggests that the metal−H_2 interaction is further weakened in the Cr(CO)$_n$-BDC complexes relative to the benzene analogues.

The calculated Cr−H_2 bond dissociation energies are shown in Table 5. As anticipated, the D_0 values for the Cr−BDC and Cr(CO)−BDC complexes (**18** and **19**) are about 3–4 kJ/mol lower than the corresponding BDC analogues **4** and **3**. For the Cr(CO)$_2$−BDC complex **20** with only one H_2 molecule interacting with the system, the interaction energy has not changed much from the corresponding **2** complex. However, the D_0 value of the −CF_3 (**23**) and −Cl (**26**) counterparts is reduced by about 10% (∼8 kJ/mol) and 15% (∼12 kJ/mol), respectively, with respect to the substituent-free system **20**. The corresponding effects of the electron-withdrawing substituents in the Cr−BDC (**21** and **24**) and Cr(CO)−BDC complexes (**22** and **25**) are not as high, with reductions on the order of 3–6% relative to the complexes **18** and **19**, respectively. Therefore, the average interaction of H_2 with the Cr metal core in the

(98) Muetterties, E. L.; Bleeke, J. R.; Wucherer, E. J.; Albright, T.A. *Chem. Rev.* **1982**, *82*, 499–525.

Table 5. Effect of Multiple Substituents: Structural Features (in pm) and the Calculated Average Cr−H_2 Bond Dissociation Energies Per H_2 Molecule (in kJ/mol) for the (X-BDC)$Cr(CO)_{3-n}(H_2)_n$ (X = −H, $-CF_3$, −Cl) Complexes

system	Cr−CO	Cr−Arene	C−O	Cr−H_2[a]	H−H[a]	D_e	D_0
			113.9[b]		75.2[b]		
4 $(C_6H_6)Cr(H_2)_3$		163.8		162.0	89.5	85.5	68.4
				162.6	88.2		
(X-BDC)$Cr(H_2)_3$							
18 H		164.0		162.6	88.5	82.4	65.0
				163.3	87.3		
21 CF_3		162.6		164.6	86.8	78.3	61.1
				164.5	85.8		
				164.5	86.6		
24 Cl		163.8		162.7	88.4	80.3	62.9
				163.8	86.7		
				164.3	86.6		
3 $(C_6H_6)Cr(CO)(H_2)_2$	183.0	166.9	117.3	162.5	88.3	88.6	71.6
(X-BDC)$Cr(CO)(H_2)_2$							
19 H	184.2	165.7	116.9	165.5	85.4	85.8	67.3
22 CF_3	185.0	164.4	116.9	166.1	84.9	81.9	63.7
25 Cl	184.3	165.7	116.8	166.0	85.1	83.8	65.4
2 $(C_6H_6)Cr(CO)_2(H_2)$	183.4	169.2	117.0	163.2	87.2	96.9	77.2
(X-BDC)$Cr(CO)_2(H_2)$							
20 H	184.4	168.8	116.6	163.4	86.9	96.5	78.1
23 CF_3	184.5	167.6	116.4	165.6	85.1	89.2	69.9
26 Cl	184.6	168.8	116.5	164.1	86.2	85.5	66.0

[a] Multiple entries refer to H1−H2, H3−H4, and H5−H6 molecules, respectively (see Figure 3 for reference). [b] Free C−O and H−H bond length (BP86/6–311G**).

BDC environment is on the order of 65–80 kJ/mol with the interaction tending to become stronger in the presence of CO ligands. With the additional help of functional groups like $-CF_3$, the H_2 binding affinity could be marginally reduced further by about 4–10 kJ/mol. From the H_2 storage perspective, this indicates that the organic linker substituent effects can tune the metal−H_2 interaction over a range of about 10 kJ/mol. However, in the context of binding energies that are up to 40 kJ/mol too strong for H_2 storage, this is simply not strong enough to effect a drastic reduction in the interaction energies. We also like to note here that the simple charge transfer interpretation explained in this section based on the changes observed in the structural geometry need not provide the complete picture. Electrostatic effects could also play an important role in influencing the trends seen in the H_2 binding interactions with various substituted Arene−metal complexes. We will investigate this notion further in section IV.

III.D Effect of the Metal Center. We have so far considered complexes that only involve the transition metal Cr. As metal−H_2 back-donation as well as H_2 sigma forward donation play a critical role in the stabilization of the metal−H_2 sigma complex, the strength of the H_2 interaction will surely be affected by the nature of the metal core as is the case with the $M(CO)_5(H_2)$ (M = Cr, Mo, W) complexes.[61,75,99] We have therefore replaced the Cr metal center in complex **4** by its iso-electronic counterparts V^- (**27**), Mn^+ (**28**), and also by the heavier Group VI element Mo (**29**). We also considered the lighter metal ions Mg^{2+} and Al^{3+} but the geometry optimization procedure yielded structures that were not valid local minima. However, the magnitude of the imaginary frequency obtained for the Mg^{2+} complex was very small ($\sim 33i$ cm^{-1}) and hence we report the corresponding results for the sake of comparison. Figure 6

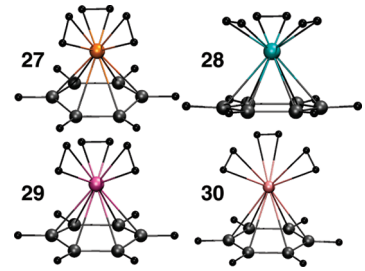

Figure 6. Optimized structures of $(C_6H_6)M(H_2)_3$ (M = V^-, Mn^+, Mo, Mg^{2+}; **27**–**30**) complexes.

displays the lowest energy configurations obtained for these complexes. Complexes **27** and **29** are quite similar to geometry obtained for complex **4**, with the exception that the benzene ring appears to be significantly distorted in the former complex. The Mn^+ analogue (**28**) appears to take up a T_d-type configuration where each H_2 molecule lies symmetrically around the metal center with its bond axis parallel to the benzene ring in a staggered conformation. The H_2 molecules arrange themselves in the same fashion as complex **4** in the Mg^{2+} complex (**30**).

The important structural features (listed in Table 6) are significantly perturbed relative to complex **4**. In the V^- (**27**) analogue, the M−Arene distance increases by about 5.5 pm, the M−H_2 distances increase by about 5–6 pm, and the H3−H4 and H5−H6 bond lengths elongate by about 5 pm relative to the complex **4**, suggesting that the metal−arene interaction and probably the forward donation of H_2 σ bonding electrons is reduced relative to complex **4**. However, at the same time the elongation of the H−H bond suggests that metal back-donation is relatively increased. This trend probably follows from the fact that the metal center is comparatively electron rich, which aids metal−H_2 back-donation and suppresses the forward donation of electrons from the H−H bond. These orbital effects are likely to cancel each other resulting in a calculated D_0 value that is only about

(99) Dapprich, S.; Frenking, G. *Angew. Chem., Int. Ed. Engl.* **1995**, *34*, 354–357.

Table 6. Effect of Transition Metal Core: Structural Features (in pm) and the Calculated Average H_2 Bond Dissociation Energies Per H_2 Molecule (in kJ/mol) for the $(C_6H_6)M(H_2)_3$ (M = V^-, Cr, Mo, Mn^+, Mg^{2+}) Complexes

M	M−Arene	M−H_2[a]	H−H[a]	D_e	D_0
			75.2[b]		
4 Cr	163.8	162.0	89.5	85.5	68.4
		162.6	88.2		
27 V^-	169.3	170.5	89.9	79.2	65.0
		167.8	93.5		
28 Mn^+	164.8	157.9	87.0	89.0	71.3
29 Mo	180.1	176.0	90.8	99.2	84.4
		174.6	92.1		
30 Mg^{2+}	203.1	217.9	76.8	50.1	41.5
		216.6	76.8		

[a] Multiple entries refer to H1−H2 and H3−H4 molecules, respectively (see Figure 2 for reference). [b] Free H−H bond length (BP86/6–311G**).

3 kJ/mol lower than complex **4**. In the Mn^+ (**28**) complex, the metal center is now less electron rich; hence, metal-back-donation to H_2 is likely to be less favored,[30,31] which could explain the shorter H−H bond length of 87 pm. At the same time, forward donation from H_2 is favored, leading to a shorter M−H_2 bond distance and higher D_0 of about 71 kJ/mol. It is also quite likely that electrostatics contributes significantly toward the interaction energies of complexes **27** and **28** because of the presence of unbalanced charges.[17,30,31]

The average D_0 calculated for the Mo complex (**29**) is 84 kJ/mol, which is about 16 kJ/mol higher than the Cr analogue (**4**). This is interesting because the M−H_2 interaction in the complexes of type $M(CO)_5(H_2)$ (M = Cr, Mo) follows the opposite trend with the Cr−H_2 interaction being stronger than the Mo−H_2 bond.[99] In the case of the half-sandwich complexes, it appears that the Mo−H_2 bond is stronger with the maximum elongation of the H−H bond length observed in this study of 92.1 pm. In the case of the Mg^{2+} (**30**) complex, the interaction of the H_2 molecules with the metal center is very weak and is most likely dominated by electrostatic charge-quadrupole and charge-induced dipole interactions. This is indicated by the weakly perturbed H−H bond length of 76.8 pm (bare "H−H" bond length at the BP86/6–311G** level is 75.2 pm) and the long M−H_2 bond distance of ∼220 pm. However, the interaction of the metal with the benzene ring is also rather weak (M−Arene bond distance ∼200 pm). Hence, replacing Cr with Mg^{2+} does not seem like a practical solution although the corresponding D_0 value for H_2 is drastically reduced to ∼35 kJ/mol. Apart from this case, the effect of changing the metal core appears to have limited success on effectively decreasing the M−H_2 interaction toward the ideal binding range from the H_2 storage point of view.

III.E Effect of Charge-Compensated Changes in the Metal Center. As we mentioned earlier, in charged complexes like **27** and **28**, the electrostatic contribution toward stabilizing the M−H_2 interaction is going to be significant. So it is interesting to investigate how the binding affinity changes when the overall charge is balanced. We therefore look at neutral complexes such as $(C_6H_6)Mn(CN)(CO)_{2-n}(H_2)_n$ (n = 1 (**31**), 2 (**32**)) and $(C_6H_6)V(NO)(CO)_{2-n}(H_2)_n$ (n = 1 (**33**), 2 (**34**)) by replacing a CO ligand with the charged isoelectronic CN^- and NO^+ analogs. We were unable to locate valid local minima for the corresponding neutral $Mg(CN)_2$ analog. The optimized geometries obtained for these complexes are shown in Figure 7. The complexes **31** and **32** are similar to the Cr-analogues **2** and **3**. However, in complex **31**, the H−H bond axis of the H_2 molecule is no longer parallel to the benzene ring but is slightly tilted toward the CN^- ligand. Similar binding characteristics are observed for the neutral V complexes **33** and **34**, with the H−H bond axis tilted away from the NO^+ ligand in complex **33**.

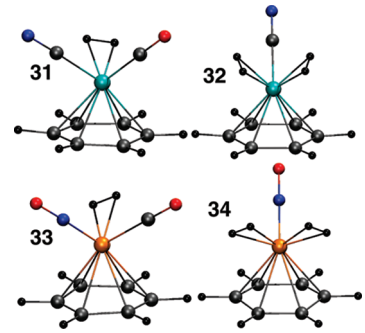

Figure 7. Optimized structures of $(C_6H_6)ML_1(L_2)_{2-n}(H_2)_n$ (M = Mn^+, V; n = 1, 2; L_1 = CN^-, NO^+; L_2 = CO; **31**−**34**) complexes.

The important structural features and the calculated average M−H_2 dissociation energy are tabulated in Table 7. The average D_0 values per H_2 molecule decreases from ∼71 kJ/mol for Mn^+ complex **28** to ∼60 kJ/mol and ∼52 kJ/mol, respectively, for the corresponding neutral Mn complexes **31** and **32**. The changes in the M−H_2 and H−H bond lengths for the complexes **31** and **32** are very small when compared to **28**. This strongly suggests that electrostatic interactions are indeed dominant in the Mn^+ complex **28**, and neutralizing the overall charge with the introduction of the CN^- ligand in complexes **31** and **32** substantially reduces that effect. A similar trend is seen with the neutral V complexes (**33** and **34**) with M−H_2 bond energies of about 60–63 kJ/mol, although the extent of decrease in the D_0 value is slightly lower than for the Mn analogues. Here, the M−H_2 and H−H bond lengths are more perturbed than for the complexes **31** and **32**. The V−H_2 bond distance is about 2–5 pm longer relative to the V^- complex **27**, while the H−H bond length is shortened by about 5–7 pm. This can be rationalized by considering that NO^+ is a good π-accepting ligand that weakens both the V−H_2 as well as the V−CO bond (∼192 pm) in complex **33**, thereby reducing the M−H_2 back-donation effects significantly. Such an effect was not observed in the Mn analogues since CN^- is a poor π-acceptor. In any case, from the context of H_2 storage, these trends are encouraging as the D_0 value can be significantly reduced. For instance, in the complex **32**, the Mn−H_2 bond energy is decreased by about 20 kJ/mol relative to the cationic Mn complex **28**.

We can expect this binding affinity to decrease further for the BDC analogue of complex **32**. Table 7 lists the corresponding features of the neutral MnCN−BDC analogue (**35**) and Figure 8 shows the corresponding optimized geometry. In accord with our expectation, the average Mn−H_2 dissociation energy (D_0) is about 48 kJ/mol, which is ∼4 kJ/mol lower than the corresponding bond energy in

Table 7. Electrostatic Effects: Structural Features (in pm) and the Calculated Average H_2 Bond Dissociation Energies Per H_2 Molecule (in kJ/mol) for the (Arene)M(L_1)(L_2)$_{2-n}$(H_2)$_n$ (M = Mn^+, V^-; n = 1, 2; L_1 = CN^-, MO^+; L_2 = CO) Complexes

system	M−L	M−Arene	L_1−L_2	M−H_2	H−H	D_e	D_0
31 (C_6H_6)Mn(CN)(CO) (H_2)	193.8[a]	163.6	117.6[a]	157.4	87.5	79.1	59.6
	178.7[b]		116.2[b]				
32 (C_6H_6)Mn(CN)(H_2)$_2$	194.1	159.9	117.7	158.8	86.5	70.6	51.8
33 (C_6H_6)V(NO)(CO)(H_2)	174.0[c]	179.2	119.4[c]	172.8	84.8	80.6	62.6
	192.0[b]		116.6[b]				
34 (C_6H_6)V(NO)(H_2)$_2$	173.1	177.2	120.0	171.5	86.0	77.7	60.2
35 (BDC)Mn(CN)(H_2)$_2$	194.4	159.6	117.5	160.2	85.5	67.7	48.2

[a] L = CN^-; L_1−L_2 = C−N. [b] L = CO; L_1−L_2 = C−O. [c] L = NO^+; L_1−L_2 = N−O.

Table 8. EDA of Representative Substituted Arene Complexes[a]

	(X−C_6H_5)Cr(H_2)$_3$			(X-BDC)Cr(H_2)$_3$	
EDA	−H (**4**)	−OCH_3 (**10**)	−CF_3 (**13**)	−H (**18**)	−CF_3 (**21**)
$-D_e$*	−118.6	−126.6	−113.0	−110.1	−103.0
ΔE_{FRZ}	116.4	108.8	113.7	117.0	110.5
ΔE_{POL}	−83.2	−78.2	−77.6	−77.1	−71.0
$\Delta E_{M\rightarrow H2\ BD}$	−63.1	−67.1	−59.5	−58.6	−53.0
$\Delta E_{H2\rightarrow M\ BD}$	−87.8	−88.9	−88.6	−90.4	−88.9
ΔE_{CT}^{HO}	3.7	3.6	3.5	3.2	3.0
E_{GD}	33.1	35.9	29.6	27.7	24.7
$-D_e$	−85.5	−90.7	−83.4	−82.4	−78.3
ΔE_{ZPVE}[b]	17.1	17.2	17.3	17.4	17.2
$-D_0$[c]	−68.4	−73.5	−66.1	−65.0	−61.1

[a] In kJ/mol per H_2 molecule; see text for definition of different terms. [b] ΔE_{ZPVE}: zero point vibrational energy correction. [c] $D_0 = D_e - \Delta E_{ZPVE}$.

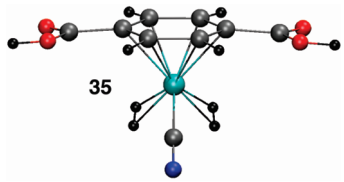

Figure 8. Optimized structure of (BDC)Mn(CN)(H_2)$_2$ (**35**) complex.

complex **32** and is consistent with the observed shorter H−H bond length (85.5 pm) and longer Mn−H_2 bond distance (160.2 pm). From our analysis on the effect of arene substituents, we could further fine-tune this Mn−H_2 interaction by introducing strong π-accepting substituents like −CF_3.

IV. Energy Decomposition Analysis

While the discussion of our results above is reasonably self-contained, it largely depends on traditional associations between structural changes and the strength of donor–acceptor interactions to explain the trends in binding energy that were seen as we altered the nature of the open metal binding sites for H_2. In this section, we attempt to dig deeper into the origin of the results using the energy decomposition analysis (EDA) to try to associate the main observed trends with particular aspects of the metal–ligand bonding, such as donor–acceptor charge-transfer interactions and electrostatic effects. We are particularly interested to see the extent to which this detailed breakdown confirms, or fails to confirm, the inferences drawn in the previous section. All results reported below use the EDA reviewed in section II.B.

IV.A Arene Substituent Effects. Table 8 provides the energy decomposition of the calculated D_e per H_2 molecule for the complex **4** and the representative π-donating and π-accepting complexes, namely, −OCH_3 (**10**) and −CF_3 (**13**). Let us first consider the absolute magnitudes of the different components of the interaction energy for the parent complex **4**. These indicate that charge transfer effects provide the roughly two-thirds of the stabilization of the metal complex H_2 interaction relative to one-third from polarization effects, while the frozen density interaction is strongly repulsive. Forward donation from H_2 to metal is in turn higher in magnitude (around 90 kJ/mol) relative to the metal back-donation effects (about 30% lower) for all the three complexes. Geometry distortion is about half the magnitude of back-donation and in the simplest interpretation is solely associated with that effect—which in turn implies that the net effect of forward donation is almost three times as large as back-donation.

Let us next consider changes in the individual energy components upon substitution. Forward donation ($\Delta E_{H2\rightarrow M\ FD}$) is relatively insensitive to the introduction of the arene substituents −OCH_3 and −CF_3while back-donation ($\Delta E_{M\rightarrow H2\ BD}$) increases by about 4 kJ/mol for the π-donating complex (**10**) and decreases by about the same amount in the π-accepting (**13**) complex. This is consistent with the rationalization provided in the previous section. The changes in the geometry distortion term are consistent with the corresponding trends in the H−H bond lengths, following our expectation that changes in the H−H bond distance with respect to its relaxed, unbound state are the major factor that determines the E_{GR} term. The π-donating complex has a strengthened interaction of H_2 with the metal core leading to an elongated H−H bond distance and therefore increased E_{GR}. The opposite occurs for the π-accepting complex.

The EDA results obtained for the BDC analogues (complexes **18** and **21**) are also tabulated in Table 8. Relative to complex **4**, the introduction of two strong π-accepting −COOH groups in complex **18** does not just lead to changes in the extent of back-donation or even charge transfer. Instead this substitution reduces the magnitude of polarization, back-donating, and geometry distortion effects by about 5–6 kJ/mol while the contribution from forward-donation from H_2 increases by about 3 kJ/mol. The net result is an overall reduction in D_e by about 3 kJ/mol for complex **18** relative to **4**. Because geometry distortion and back-donation are directly coupled, this EDA suggests that the overall decrease is best regarded as being due to changes in electrostatic effects. This is not the picture we relied on in the previous section.

Roughly similar trends are observed in the −CF_3 complex **21** relative to complex **13**. In this case, forward donation is largely unchanged while back-donation is reduced by about 7 kJ/mol; and polarization, by nearly the same. The decrease

Table 9. Energy Decomposition Analysis (EDA) of $(C_6H_6)M(H_2)_3$ (M = V^-, Cr, Mo, Mn^+, Mg^{2+}) Complexes[a]

EDA	Cr (**4**)	V^- (**27**)	Mn^+ (**28**)	Mo (**29**)	Mg^{2+} (**30**)
$-D_e$*	−118.6	−130.3	−115.8	−143.3	−45.4
ΔE_{FRZ}	116.4	139.6	138.8	123.9	13.3
ΔE_{POL}	−83.2	−119.3	−85.3	−85.6	−13.6
$\Delta E_{M\rightarrow H2\ BD}$	−63.1	−88.7	−47.1	−74.9	−1.4
$\Delta E_{H2\rightarrow M\ BD}$	−87.8	−64.8	−122.1	−107.1	−47.7
ΔE_{CT}^{HO}	3.7	6.8	5.6	3.4	3.8
E_{GD}	33.1	51.1	26.7	44.1	1.4
$-D_e$	−85.5	−79.2	−89.1	−99.2	−44.0
ΔE_{ZPVE}[b]	17.1	14.2	17.7	14.8	8.6
$-D_0$[c]	−68.4	−65.0	−71.4	−84.4	−35.4

[a] In kJ/mol per H_2 molecule; see text for definition of different terms. [b] ΔE_{ZPVE}: zero point vibrational energy correction. [c] $D_0 = D_e - \Delta E_{ZPVE}$.

in the polarization and back-donation terms is partially offset by the geometry distortion effects leading to an overall reduction of 5 kJ/mol in the D_e and D_0 values. Since geometry distortion and back-donation are directly coupled, this again suggests that the net decrease in binding in **21** relative to **13** is best viewed as a net change in electrostatic interactions, with only a marginal net contribution from the change in back-donation.

IV.B Effect of Metal Center. In Table 9, the EDA results obtained for the various metal complexes **27**−**30** are listed along with that of complex **4**. In absolute terms, the donor–acceptor interactions remain the dominating effect toward stabilizing the metal−H_2 interaction for all the cases considered. Forward donation ($\Delta E_{H2\rightarrow M\ FD}$) is stronger than metal-back-donation in all cases except for the V^- complex (**27**). In complex **27**, the back-donating abilities of the highly electron-rich V metal center are increased while at the same it becomes more reluctant to accept electron density from the H−H bonding orbital. The ΔE_{FRZ}, ΔE_{POL}, and ΔE_{GR} components are also significantly perturbed in this case relative to complex **4**. However, these effects nearly cancel, leading to a marginal overall decrease in the binding energy.

For the Mn^+ complex (**28**), $\Delta E_{H2\rightarrow M\ FD}$ is about 35 kJ/mol higher than for the Cr−complex (**4**) while $\Delta E_{M\rightarrow H2\ BD}$ is decreased by about 17 kJ/mol. This is consistent with the electron poor metal center in the Mn-complex (**28**) promoting forward donation from H_2 while metal back-donation is reduced.[30,31] The strong forward donation is only partially canceled by increases in the ΔE_{FRZ} and ΔE_{GR}, leading to an overall increase in D_e and D_0 relative to complex **4**. We also note here that the higher order relaxation component (ΔE_{HRLK}) of the decomposition in the case of both the V^- (**27**) and the Mn^+ (**28**) complexes are higher (almost double) than the other complexes considered, indicating that the overestimation of the charge transfer components by perturbation theory is relatively greater in these systems.

In the case of the Mo-complex (**29**), all the components of the EDA are higher relative to the Cr-complex (**4**) leading to higher H_2 binding affinities. Combining ΔE_{GR} and $\Delta E_{H2\rightarrow M\ FD}$ shows that the net change due to back-donation is relatively small, and the key change is in $\Delta E_{H2\rightarrow M\ FD}$. The EDA of the only nontransition metal case considered, the Mg-complex (**30**), indicates that the metal center is almost incapable of back-donation to H_2. While forward donation is only about half as large as for transition metals, this is now decisive because electrostatic effects have changed very strongly to yield no net repulsion. In an absolute sense, we have the perhaps surprising result that forward donation is largely responsible for the overall binding.

Table 10. EDA of Representative Neutral Metal (Mn, V) Complexes[a]

EDA	$(C_6H_6)Mn(CN)(H_2)_2$ (**32**)	$(BDC)Mn(CN)(H_2)_2$ (**35**)	$(C_6H_6)V(NO)(H_2)_2$ (**34**)
$-D_e$*	−98.6	−93.9	−100.8
ΔE_{FRZ}	134.5	132.9	77.9
ΔE_{POL}	−74.9	−72.3	−51.6
$\Delta E_{M\rightarrow H2\ BD}$	−51.1	−46.4	−53.8
$\Delta E_{H2\rightarrow M\ BD}$	−108.9	−110.1	−73.6
ΔE_{CT}^{HO}	3.7	3.6	2.6
E_{GD}	28.0	26.2	23.2
$-D_e$	−70.6	−67.7	−77.7
ΔE_{ZPVE}[b]	18.8	19.5	17.5
$-D_0$[c]	−51.8	−48.2	−60.2

[a] In kJ/mol per H_2 molecule; see text for definition of different terms. [b] ΔE_{ZPVE}: zero point vibrational energy correction. [c] $D_0 = D_e - \Delta E_{ZPVE}$.

IV.C Neutral Metal Complexes. Table 10 lists the EDA obtained for the neutral V (**34**) and Mn (**32**, **35**) complexes considered. In the neutral V complex (**34**), ΔE_{FRZ} and ΔE_{POL} are reduced by 44% and 56%, respectively, relative to the anionic analog (**27**), causing an overall reduction in binding of about 5 kJ/mol due to electrostatics. Charge-transfer effects in **34** are reversed relative to complex **27**, with $\Delta E_{H2\rightarrow M\ FD}$ dominating as expected from charge neutralization. The strong reduction in back-donation is associated with an almost 50% reduction in the geometry distortion term.

In case of the neutral Mn complexes (**32**), the changes in the FRZ, POL, and GR terms relative to its cationic analogue (**28**) are much lower compared to the V-complexes. The large decrease observed in D_e* appears to stem primarily from the lowering of the $\Delta E_{H2\rightarrow M\ FD}$ by about 13 kJ/mol relative to **28**. With the overall neutralization of the charge on the complex, the metal center is now less electron poor, thereby decreasing its electron accepting ability. Relative to the parent complex, **4**, the most striking change is in overall electrostatics, which become far more repulsive at the optimized geometry, with the net increase outweighing the strengthening of (attractive) forward donation. Similar effects are found in the BDC analogue of the Mn complex (**35**).

V. Conclusions

In this computational study, we have systematically investigated the nature and strength of 35 sigma-bonded transition metal−dihydrogen complexes of the type (η^6-Arene)$M(L1)_{n1}(L2)_{n2}(H_2)_{3-n1-n2}$ using density functional theory. The predicted structural features of these systems were found to be consistent with experimental studies on the analogous (η^6-Arene)$Cr(CO)_3$ (**1**) complexes.[50,58] The estimated average dissociation energies D_0 for the reported complexes range between 48 and 84 kJ/mol.

The observed trends in the interaction energies could be correlated to the electronic effects of the arene substituents, the ligand environment, and the metal core. The EDA clearly reflected the sensitivity of the M−H_2 bond strength toward the extent of donor–acceptor interactions, especially metal back-donation to the H_2 molecule. For instance, we found that the presence of strong π-accepting arene substituents

like $-CF_3$, that are also good electron-withdrawing groups, tend to marginally weaken the $M-H_2$ interaction. This effect could be further enhanced in the presence of multiple electron-withdrawing groups like $-COOH$ in the M−BDC complexes.

EDA shows that correlations between binding energies and features of structure like H−H distance in all likelihood oversimplify the origin of trends in hydrogen binding affinities. Detailed analysis shows that changes in electrostatic effects are perhaps the most significant determinant of both arene substituent effects and the overall reductions in binding energy (∼20 kJ/mol) achieved by the charge-compensated $(BDC)Mn(CN)(H_2)_2$ complex. But just as net binding emerges from partial cancelation between a variety of terms whose magnitudes are relatively large in comparison to the binding energy itself, it is also difficult to attribute substituent-induced shifts solely to a single component of the binding energy.

From the perspective of improving the H_2 sorption characteristics of MOFs at room temperature, the incorporation of transition metal groups like $Cr(CO)_3$ onto organic linkers like BDC gives much stronger binding than the weak, dispersion dominant H_2 interaction with BDC itself. In fact, the range of the calculated transition metal−dihydrogen binding affinity appears to be a little too strong for easy desorption under ambient conditions (ideally, it should range between 20 and 40 kJ/mol). With our systematic study of possible control factors, we have shown that the $M-H_2$ binding strength could be fine-tuned by introducing strong π-acidic arene substituents. The largest decrease in the $M-H_2$ affinity was, however, observed in the $(BDC)Mn(CN)(H_2)_2$ (**35**) complex, where the electrostatic interactions were greatly reduced by charge neutralization. We also note here that a very recent theoretical study[100] estimates the H_2 binding affinity obtained with lighter transition metals like Sc and Ti, in place of the heavier transition metal complexes (such as **4** and **29**) studied in this paper, to be in the range of about 40–60 kJ/mol. This is an encouraging indication as we could potentially push the H_2 binding energy into the ideal binding regime by further taking into account arene substituent effects. We are currently investigating this possibility and hope to report our findings in the near future.

Acknowledgment. This work was funded by the Department of Energy through Grant DE-FG36-05GO15002 with additional indirect support from the Department of Energy through the Computational Nanosciences program for the development of relevant methodology. We thank Jeffrey R. Long, Steven S. Kaye, and Mircea Dinca for useful discussions.

Supporting Information Available: Cartesian coordinates of all reported optimized structures and their calculated absolute energies (PDF). This material is available free of charge via the Internet at http://pubs.acs.org.

IC701625G

(100) Weck, P. F.; Dhilip Kumar, T. J. *J. Chem. Phys.* **2007**, *126*, 094703.